Appl Petrochem Res (2014) 4:189–207
DOI 10.1007/s13203-013-0038-6

ORIGINAL ARTICLE

The time-on-stream stability of some selected bifunctional nanoporous-based catalysts in *n*-heptane hydroisomerisation

Faisal M. Alotaibi · Raed H. Abudawood · Hamid A. Al-Megren · Mohammed C. Al-Kinany · Arthur A. Garforth

Received: 29 August 2013 / Accepted: 25 October 2013 / Published online: 27 November 2013

Abstract In this work, some commercial nanoporous-based catalysts, such as USY, beta and mordenite zeolites loaded with Platinum metal acting as bifunctional catalysts, were used for hydroisomerisation experiments in a fixed-bed reactor at the atmospheric pressure and at feed space time 5.12 h^{-1} to hydroisomerise *n*-heptane over a temperature range of 210–270 °C. The study aimed to evaluate the changes with time-on-stream in the catalytic activity, product selectivity and manner of deactivation of metal-loaded zeolite catalysts, at constant contact time of 5.13 h^{-1} and a hydrogen-to-*n*-heptane molar ratio fixed at 9. Various analytical techniques were used to characterise fresh and aged catalysts. Results show that pore architecture is the most important factor affecting coke formation and deactivation in zeolite catalysts, and those catalysts with three-dimensional pore structures lacking cavities or cages were best able to resist deactivation. In addition, it was found that those catalysts with high Si/Al ratios and those which had been acid-leached or steamed showed better activity, higher selectivity towards isomeric products and better time stability. Moreover, the balance between the number of metal sites and the number of acid sites played an important role in determining the activity, selectivity and stability of the bifunctional catalysts.

Keywords The time-on-stream stability · Alkanes hydroisomerisation · Catalyst deactivation · Zeolites · Bifunctional catalysts · Nanoporous catalysts

F. M. Alotaibi (✉) · H. A. Al-Megren · M. C. Al-Kinany
Petrochemicals Research Institute, King Abdulazeez City for Science and Technology (KACST), PO Box: 6086, Riyadh 11442, Saudi Arabia
e-mail: alotaibi1975@gmail.com; fmsalotaibi@kacst.edu.sa

R. H. Abudawood
Research and Development Center Saudi Aramco, Dhahran 31311, Saudi Arabia

A. A. Garforth
School of Chemical Engineering and Analytical Science, The University of Manchester, Manchester M13 9PL, UK

Introduction

Catalysts that are being tested for industrial processes must adhere to strict criteria for the reaction which is being targeted. For example, they need to have high levels of both activity and selectivity, together with a long period of stability. One of the most common problems which occur is deactivation at some point during the process, which can reduce the levels of activity, of selectivity, or of both. One of the possible contributory causes is carbonaceous deposits over the catalyst, which is quite common in hydrocarbon conversion processes. The type of catalyst, in conjunction with the reaction conditions, will affect the success of the catalyst. Its lifetime is a crucial feature when working with zeolites, and extending the catalyst lifetime from minutes to days will improve success rates dramatically [1, 2]. The cost of catalyst deactivation is very high in industrial processes; therefore, catalysts with superior time stability are very valuable. Large pore zeolites, especially high-silica zeolites, are attractive catalysts for reforming-type reactions, and the time stability of these catalysts would be one of the important factors in determining their use in such reactions [2].

Despite extensive studies over the last 20 years into the formation and nature of coke on zeolites, there is still much discussion and controversy on many questions. Rollmann and Walsh were among the first to show that coke

formation is a shape-selective reaction. They noted that coke yield in molecular shape-selective zeolites (small and intermediate pore) is at least an order of magnitude lower than in the large pore materials [3, 4]. However, the effect of zeolite pore structure is concerned with more than just steric restrictions on the formation of coke precursors. The contact time of the organic molecule with the active sites is determined by the rate of diffusion of these molecules and therefore by the characteristics of the diffusion path inside the zeolite crystallites: the length related to the crystallite size, the size of the pore apertures, the size of the channel intersections and the acid site density. The choice of pore structure of the zeolite must therefore ensure that the spaces in the vicinity of the acid sites are big enough to permit the intermediates of the desired reaction to form yet small enough to limit the formation of coking intermediates by strict constraints. In addition, the diffusion of the desirable molecules must be quick enough for the reactant transformation to be restricted to the formation of the desired product [5, 6]. The study by Gopal and Smirniotis demonstrated that three-dimensional zeolites without supercages, such as zeolite beta, when they have the correct level of acid site density and metal loading, are ideal catalysts for reforming-type reactions, due to their time stability. Catalyst performance was greatly affected by acid site density and the researchers were able to identify an optimum range for obtaining good stability [2, 7]. Zhang and Smirniotis found that the zeolite pore structure played a very important role in the reforming of industrial naphtha (rich in naphthenes) and that an appropriate combination of the zeolite pore structure and its acidity, controlled via dealumination, gave superior time-on-stream stability for the reactions investigated. Thus, zeolites with channel intersections (cavities) of comparable size with the zeolite apertures did not favour coke formation. Therefore, they found that the dealuminated ZSM-12 demonstrated unique TOS stability for reforming types of reactions and concluded that this behaviour resulted from (a) its pore structure, which does not favour coke formation, and (b) the balance of its acidity. In terms of the zeolite structure and its effect on coke formation, there are two extreme cases, in the first case, coke precursors can be trapped and enlarged in the supercages, resulting in a blocking of the pores, since the zeolite has relatively large cavities or supercages in comparison with the opening of the channels. Whereas for the other type of zeolites, the channel intersection is comparable in size with the opening of the zeolite aperture, making it difficult for coke precursors to accumulate and form further large molecules in the channel, because of the space constraint [8]. The effects of acidity and of the pore structure are difficult to tell apart, but as a rule, zeolites with higher acid site densities deactivate faster as a result of higher conversion severity, which ultimately gives higher coke yields. In reforming reactions, when carried over bifunctional catalysts, the coke precursors are hydrogenated over the metal function and become desorbed. This is advantageous because the coke production rate is much lower than that over an acidic catalyst [9].

At present, as new gasoline standards require the content of aromatics and olefins to be reduced, the hydroisomerisation of paraffins with chain lengths above C6 is extremely advantageous. For this reason, much research has been done to find effective catalysts which can encourage the selectivity of branched paraffins in the hydroisomerisation of these paraffins. *n*-C7 is one of the most important fractions of naphtha; due to its low octane number, it is separated and diverted to a continuous catalyst regeneration (CCR) unit, where hydrocracking occurs under severe conditions, resulting in the production of some light gaseous hydrocarbons. Thus, the hydroisomerisation of *n*-C7 to mono- and multibranched isomers is an important area which merits research. The reactions of hydrocarbons over acidic zeolite catalysts are accompanied by the formation of coke, which causes catalysts to deactivate and leads to changes in product distribution [10–13].

In this work, the time-on-stream (TOS) behaviour and deactivation rates of some commercial USY, beta and mordenite zeolites that have been loaded with Platinum metal, with a wide range of Si/Al ratios, pore sizes and acidity characteristics, are evaluated in the hydroisomerisation of *n*-C7 when reaction conditions such as temperature, pressure and contact time are varied. *n*-C7 was used as a representative model compound for naphtha. A range of techniques was used to characterise fresh and aged catalysts under the conditions of each reaction.

Experimental

Catalyst preparation

Some commercial USY, beta, and mordenite samples were provided by different suppliers [14–18], as shown in Table 1. These zeolite supports were designed and modified by various post-synthesis techniques so that they could be used for multiple purposes; for instance, high alkane hydroconversions such as cracking, isomerisation and alkylation. They were supplied in powder form without binder materials.

The catalysts listed in Table 1 were loaded with 1 wt% platinum via the ion exchange technique in their ammonium form using an amino complex of platinum. This technique was used by Weisz and Frillete [19] to exchange platinum into zeolite A. In the loading procedure, 1 g of each catalyst in the ammonium form was mixed with 0.0175 g of

Table 1 List of catalyst supports investigated in the TOS study

	Zeolite trade name	Zeolite type	Post-synthesis modification applied	Supplier
1	CBV712	USY	Steamed and acid-leached	Zeolyst International
2	CBV720	USY	Severely steamed and acid-leached	Zeolyst International
3	USY-A	USY	Mildly steamed	Crosfield
4	CP814E	BEA	As-synthesised	Zeolyst International
8	CBV21A	MOR	As-synthesised	Zeolyst International
9	640HOA	MOR	Mildly steamed and acid-leached	Tosoh Corporation
10	660HOA	MOR	Moderately steamed and acid-leached	Tosoh Corporation
11	690HOA	MOR	Severely steamed and acid-leached	Tosoh Corporation

tetramine platinum (II) chloride $[Pt(NH_3)_4Cl_2{\cdot}H_2O]$ (Aldrich, 99.5 % purity), and dissolved in 50 ml of deionised water, then the pH of the mixture was adjusted to more than 9 by adding ammonia solution (32 %, Aldrich) such that it resulted in 1 wt% platinum loading on the zeolite sample, assuming a complete uptake of platinum in the catalyst. The mixture was left stirring at room temperature for 24 h, after which it was centrifuged and washed with 10 times its volume of deionised water to ensure that the catalyst would be free of any residual chloride ions. The washed catalyst was then dried overnight at 110 °C. Elemental analysis was used to confirm loadings at 1 wt% and that the samples were free of chloride ions.

Catalyst characterization

Characterization techniques used were: ICP optical emission spectroscopy (ICP-OES), X-ray diffraction (XRD), ^{27}Al and ^{29}Si MAS-solid-state NMR, pyridine adsorption Fourier transform infrared spectroscopy, ammonia temperature programmed desorption (NH_3-TPD), scanning electron microscopy and energy dispersive X-ray analysis (SEM), transmission electron microscopy (TEM), X-ray photoelectron spectroscopy (XPS), hydrogen chemisorption of platinum, BET surface area analysis by nitrogen adsorption, and thermogravimetric analysis (TGA).

Catalyst loading and activation

Catalysts were pelletized and sieved to obtain particles in the size range of 250–420 μm prior to loading into the reactor. A sample (1 g) of catalyst was sandwiched in the reactor between two layers of inert glass beads held in place by glass wool to form the catalytic bed. The catalyst was activated in situ by first removing ammonium via calcination with flowing air (50 ml min^{-1}) at 500 °C for 2 h at a heating rate of 3 °C min^{-1}. Following the removal of the ammonium, the catalyst was then reduced in a hydrogen (100 ml min^{-1}) atmosphere at 450 °C for 4 h, which resulted in the conversion of platinum ions into their metallic form. As fast heating rates can cause agglomeration of platinum ions, which leads to a poor catalyst performance, a slow temperature ramping rate of 3 °C/min was used during calcination.

Catalyst testing

n-Heptane (*n*-C7) with >99 % purity (Sigma-Aldrich) was fed to the catalyst bed using an HPLC pump, and hydrogen of high purity was introduced to give an H_2/*n*-C7 molar ratio of 9. The deactivation behaviour of zeolite catalysts was investigated during the catalytic conversion of *n*-C7 at reaction temperatures of 210, 230, 250 and 270 °C, with fresh catalyst was used for each run at each of the reaction temperatures and at atmospheric pressure using the glass fixed-bed flow reactor system loaded with 1 g of 1 % Pt loaded catalyst, and weight hourly space velocity (WHSV) was 5.13 h^{-1}.

Most of the deactivation runs for each catalyst lasted for at least 5 days. All gas and liquid samples were collected once a day, except in some cases where the sample could be collected more frequently. Gas samples were collected in a 1-L gas bag and the gas outlet flow rate was measured regularly using a bubble meter in order to perform a mass balance on the unit. The liquid samples collected were analysed by injecting 0.1 μL into a Varian 450 GC. After each reaction, the reactor was reduced to ambient temperature and purged with nitrogen overnight to remove any residual *n*-C7. The used or spent catalysts were collected after the reaction and stored in sealed containers for further analysis. Products were analyzed using a Varian 450 GC equipped with a 50 m × 0.32 mm i.d. PLOT Al_2O_3/KCl capillary column fitted to an FID detector for gas products and a CP-Sil PONA CB optimised gasoline column fitted to an FID detector for liquid products.

Results and discussion

Deactivation behaviour of CBV712 USY zeolite

CBV712 USY is produced via mild acid leaching of CBV600 USY which is prepared by steaming of CBV300 (Na-Y) as the starting material and which has been ammonium-exchanged for over 80 % [20]. Figures 1 and 2 show, respectively, the XRD pattern and SEM micrograph of CBV712 USY.

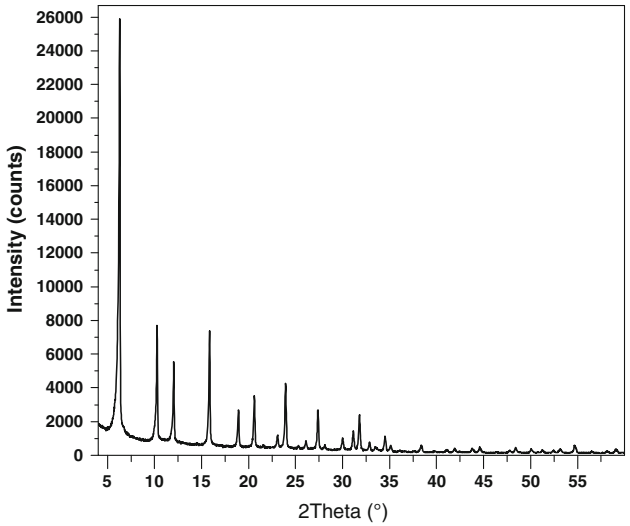

Fig. 1 XRD pattern of CBV712 USY

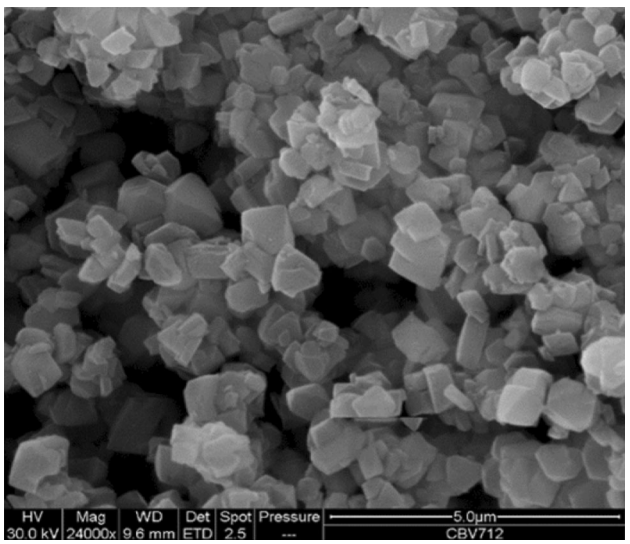

Fig. 2 SEM micrograph of CBV712 USY

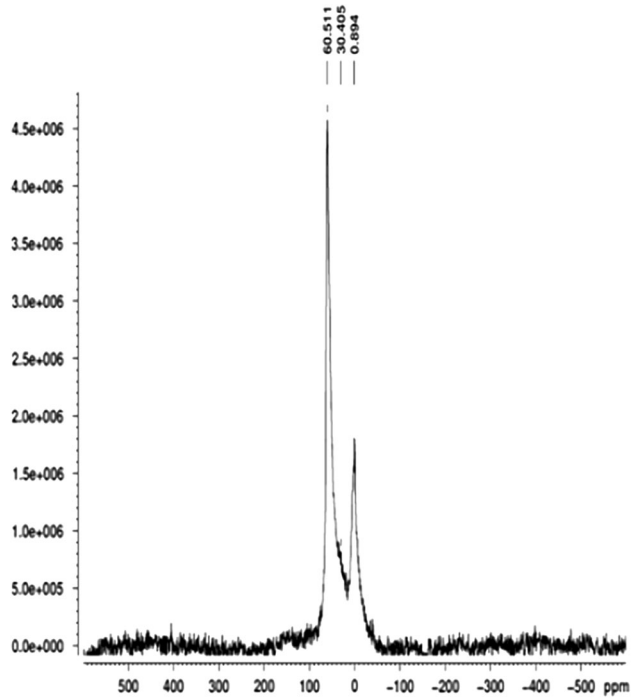

Fig. 3 ^{27}Al MAS NMR spectra of CBV712

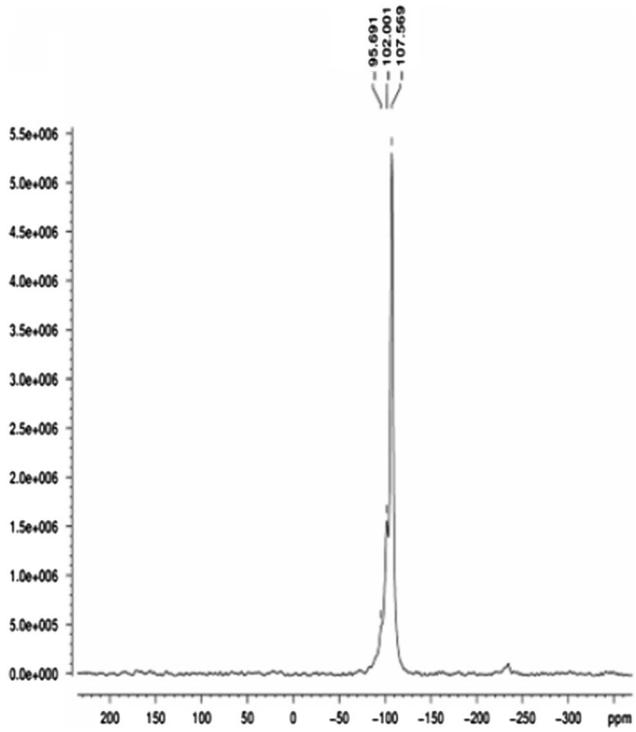

Fig. 4 ^{29}Si MAS NMR spectra of CBV712

The XRD pattern is consistent with that reported in the literature for ultrastable zeolite Y phase [21], thus confirming the USY phase. The SEM image shows sharp-edged cubic crystallites of zeolite Y phase. These varied in size from 1 to 3 μm and were combined with an amorphous phase which normally surrounds the zeolite Y crystals after the dealumination process. This may be a consequence of the acid leaching treatment which followed dealumination and resulted in USY zeolite with less extra-framework aluminium (EFAL) species (the amorphous phase).

Figures 3 and 4 show solid-state NMR spectra for ^{27}Al and ^{29}Si, respectively. In ^{27}Al MAS NMR analysis of the fresh CBV712 USY sample, as delaminated and partially acid-leached zeolites, Fig. 3 shows unique resonance spectra for three different chemical environments of aluminium. The first environment is assigned to in-framework aluminium in tetrahedral coordination $Al(OSi)_4$ with a chemical shift of approximately 60 ppm. The second

Table 2 In-house characterisation of CBV712 USY

	Before ion exchange				After ion exchange with Pt precursor as tetramine platinum (II) chloride $(Pt(NH_3)_4Cl_2)\cdot H_2O$			
Elemental analysis (bulk)	Si/Al mole ratio		5.93		Si/Al mole ratio	5.93	Pt wt%	0.98
XPS[a] atomic % conc	Si	Al	Si/Al	Pt	Pt was found in its metallic form on the surface			
	26	4.27	6.09	0.04				
XRD	Crystallinity				Related to in-house as-synthesised Y			
	87.50							
NMR	Si/Al mole ratio for the framework				Three chemical environments for Si-NMR: Si(0Al), Si(1Al), and Si(2Al)			
	8.34				Lewis acid sites are existed: $Al(OSi)_4$, $(Al(H_2O)_5)^{3+}$, and $(Al(H_2O)_6)^{3+}$			
Ammonia TPD[b]	NH_3 desorption through TPD/mmol g^{-1}				Ammonia adsorption calorimetry followed by temperature programmed desorption			
	0.70 (±0.01)							
Hydrogen chemisorption[b]	Metal dispersion %		Metallic surface area $m^2\ g^{-1}$ metal		Metallic surface area $m^2\ g^{-1}$ sample		Crystallite size nm	
	38.44		94.95		0.93		2.95	
BET[b]	Surface area $m^2\ g^{-1}$		Pore volume $cm^3\ g^{-1}$		Pore size Å		Shows both micro and mesoporosity	
	816.26		0.45		42.75			
TGA for coke content in spent catalyst (mass loss wt% in air) after various reaction temperatures	210 °C		Top	0.30	250 °C		Top	1.47
			Mid	0.12			Mid	1.26
			Bot	0.12			Bot	0.88
	230 °C		Top	0.23	270 °C		Top	4.89
			Mid	0.17			Mid	4.78
			Bot	0.12			Bot	4.87

[a] LPD Laboratory Services Ltd.

[b] MCA Services

environment is assigned to the five-coordinated EFAL with a chemical shift of about 30 ppm. The third environment is assigned to non-framework aluminium in octahedral coordination with a chemical shift of around 0 ppm. Information about the Si atoms coordinated (via oxygen) with neighbouring T atoms (Si, Al) is provided by ^{29}Si MAS NMR. Figure 4 shows the ^{29}Si MAS NMR spectra of CBV712 USY. The ^{29}Si MAS NMR spectrum exhibits peaks at around −107, −102 and −95 ppm which were assigned to different configurations of SiO_4 (4Si,0Al), SiO_4 (3Si,1Al), SiO_4 (2Si,2Al), respectively. Table 2 shows the in-house characterisation of CBV712 USY using various techniques.

Figure 5a–d illustrates the effects of TOS on the C7 conversion, hydroisomerisation, hydrocracking and cyclic product yields at reaction temperatures ranging from 210 to 270 °C.

Initially, 30 min after introducing the feed to the reactor at temperatures of 210, 230, 250 and 270 °C, the overall conversion was 20, 47, 75 and 88 wt%, respectively. At the lowest temperature of 210 °C, the catalyst initially lost about 3 wt% of its activity, then, after 60 h on stream, a constant value was achieved. On the other hand, the deactivation rate at 230 °C for the fresh catalyst was slightly more rapid, as shown in Figs. 4, 5 and 6a. The overall conversion 30 min after introducing the feed to the reactor was 47 wt%, which decreased after 240 min on stream to 45 wt%, then decreased slowly, with the deactivation rate ranging between 2 and 4 wt% every 24 h until the reaction terminated after about 3 days (4,440 min). At the higher temperatures of 250 and 270 °C, it showed a rapid fall in catalyst activity during the initial few hours, followed by a constant deactivation rate being reached, which ranges from 3 and 5 wt% every 24 h until the reaction terminated.

Selectivity towards the hydroisomerisation products ranged from 99 to 100 % during the deactivation run at the lower temperatures of 210 and 230 °C, from the introduction of the feed to the reactor until both reactions terminated. On other hand, selectivity towards cracked and cyclic products was very low and fluctuated in a very narrow range of 0.5 %, as a function of TOS. The initial selectivity towards the hydroisomerisation products was 95 and 77 % at 30 min after introducing the feed to the reactor, which increased throughout the TOS to 98 and 97 wt% after 720 min at temperatures of 250 and 270 °C,

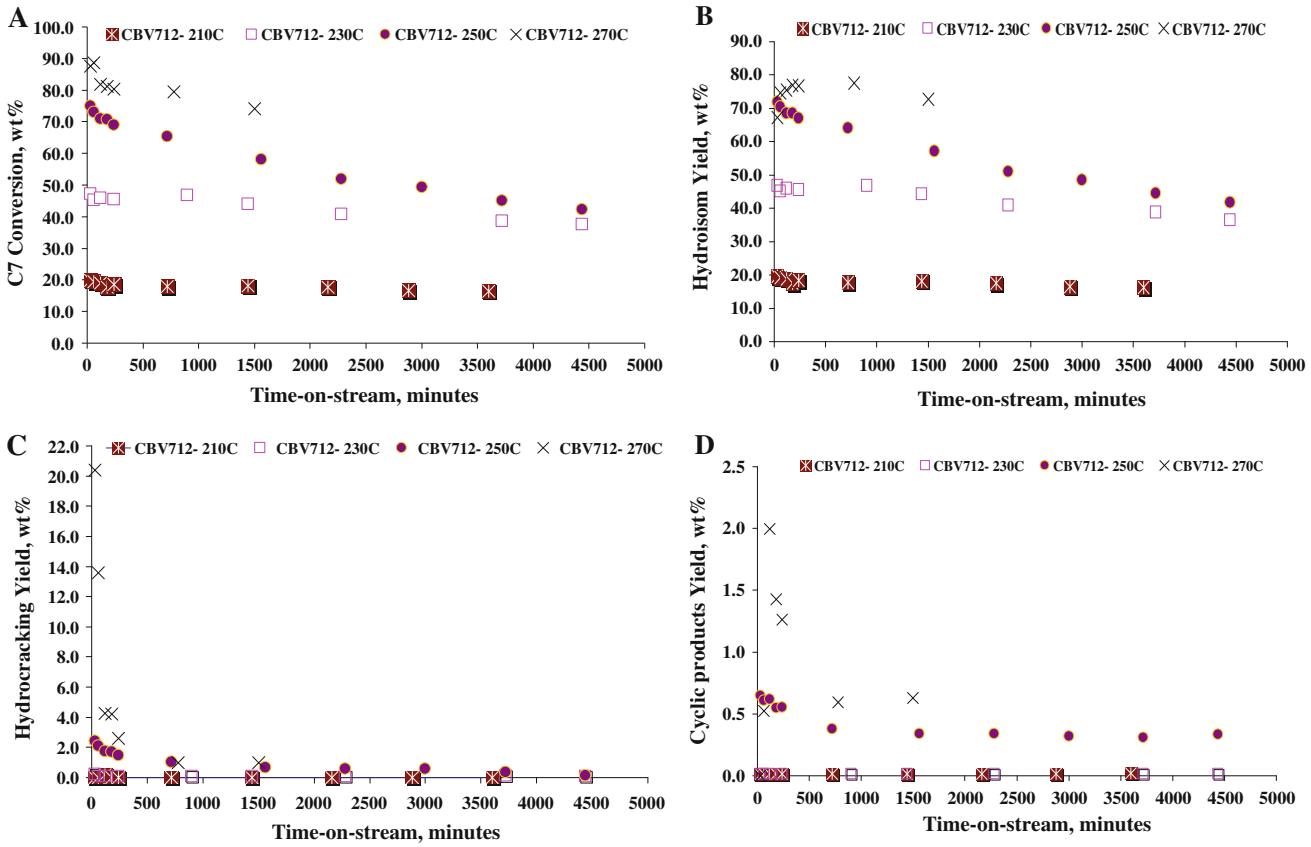

Fig. 5 Overall conversion (**a**), total yield of C7 isomers (mono + di + tribranched isomers) (**b**), total hydrocracking yield (**c**), and total yield of the cyclic products (**d**) as a function of TOS for CBV712 USY at various reaction temperatures. WHSV = 5.13 h^{-1}; H_2/C7 (mol/mol) = 9; total pressure = 1 atm; temperature = 210, 230, 250 and 270 °C; 1 wt% Pt loading

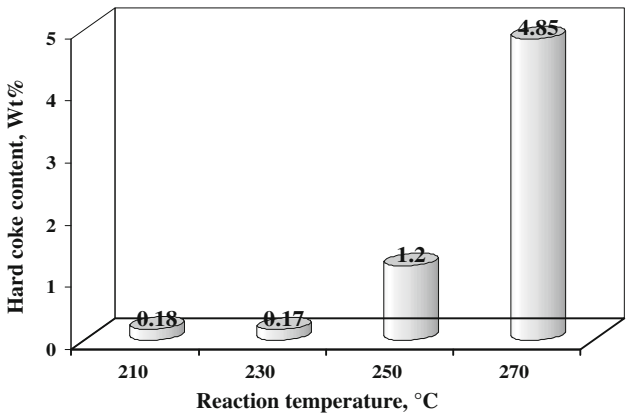

Fig. 6 Average hard coke content over the aged CBV712 USY bed

respectively. Meanwhile, selectivity towards cracked products was quite high at the higher temperatures during the initial few hours of the deactivation reaction. The highest cracked product selectivity was 23 % at 270 °C, 30 min after the introduction of the feed to the reactor, after which it decreased rapidly throughout the TOS to 3 wt% after 240 min. The yield of cyclic products at 250 and 270 °C was higher than at lower temperatures.

It can be observed that the total conversion increased dramatically when increasing reaction temperature in the range of 210–270 °C, with the maximum isomer yield obtained with the CBV712-based catalyst was around 77 wt% at 270 °C, with the predominant conversion being hydroisomerisation. However, the selectivity for C7 isomers at lower temperatures was very high throughout the deactivation reactions of 210 and 230 °C, yielding a greater proportion of branched C7 as a result of the thermodynamic equilibrium. The selectivity of cracked products initially increased at higher temperatures (250–270 °C) during the first few hours of the deactivation reaction, then decreased rapidly throughout the TOS, whereas the selectivity of cyclic products was slightly higher at 250 and 270 °C than at the lower temperatures of 210 and 230 °C.

The CBV712 was steamed and acid-leached to ensure the microporosity and mesoporosity of the networks within its structure; resulting in a high surface area and pore volume, as shown in Table 2. This resulted in a rapid loss in C7 hydroisomerisation conversion activity with TOS, particularly at higher temperatures, that can be explained

by considering the Brønsted and Lewis acid sites of the CBV712. The Brønsted acidity is predominant, with acid sites within its structure being stronger, resulting in the majority of the aluminium ions incorporated in a tetrahedral coordination, as seen in the ^{27}Al MAS NMR and TPD analysis. In addition, it can be concluded that the catalyst CBV712 has a high acid site density and a mild strength of acidity due to the existence of both types of acid sites, resulting in the catalyst exhibiting high activity, particularly at higher temperatures, resulting in increased activity for the cracked products as coke precursors in the initial few hours of the deactivation run, ultimately leading to coke formation, which preferentially deactivated the strongest acid sites which contribute to the cracking reaction.

Figure 6 shows the TGA results of the average of the hard coke content deposited over the top, middle and bottom zones of the aged CBV712 USY catalyst bed after unloading the spent catalyst from the atmospheric glass reactor. It can be clearly seen that the top zones had the highest hard coke content in the catalyst bed at each reaction temperature, whereas there was slightly less coke in the middle and bottom zones. This suggests that the top zone of the catalyst bed contributed the most activity and was where the reaction took place. In addition, the high coke content in the top zone is to some extent indicative of the high acidity of this catalyst, affecting its stability and thus increasing the rates of deactivation and coking. It is evident that there is a clear correlation between the temperature and the yield of cracked products obtained, which relates to the existence of stronger acid sites and to the hard coke content deposited in the catalyst cages at different reaction temperatures. The maximum hard coke value of 4.85 wt%, which was found at the highest reaction temperature of 270 °C, was 27 times higher than that at the lower temperatures of 210 and 230 °C.

Research has shown that the ratio between the number of Pt atoms (n_{Pt}) and the number of acid sites (n_A) plays an important role in determining the activity, selectivity and stability of the bifunctional catalyst, which must be well-balanced to behave as an 'ideal' hydroconversion catalyst. It has been found that the optimum limits for the n_{Pt}/n_A ratio range between 0.03 and 0.17, and the greater the value of n_{Pt}/n_A, the smaller the number of chemical steps by which the cracked products can be generated and then oligomerated to form the coke molecules, hence, the slower the coke formation and the higher the catalyst stability [22–24]. The n_{Pt}/n_A ratio for CBV712 was calculated to be 0.072, which is within the optimum limits specified above, although its time stability was not quite as good at 250 and 270 °C. A possible explanation for this is that the above suggestion is not empirical in all reaction conditions and that it can be proven that CBV712 did not behave as an ideal hydroconversion catalyst at higher temperatures,

Table 3 In-house characterisation of CBV720 USY

	Before ion exchange				After ion exchange with Pt precursor as tetramine platinum (II) chloride $(Pt(NH_3)_4Cl_2).H_2O$			
Elemental analysis (bulk)	Si/Al mole ratio		14.99		Si/Al mole ratio	14.99	Pt wt%	1.08
XPS[a] atomic % conc	Si	Al	Si/Al	Pt	Pt was found in its metallic form on the surface			
	28.55	1.76	16.22	0.02				
XRD	Crystallinity				Related to in-house as-synthesised Y			
	92.12							
NMR	Si/Al mole ratio for the framework				Two chemical environments for Si-NMR: Si(0Al) and Si(1Al)			
	31.2				Two Lewis acid sites existed: $Al(OSi)_4$ and $(Al(H_2O)_6)^{3+}$			
Ammonia TPD	NH_3 desorption through TPD/ mmol g^{-1}				Ammonia adsorption calorimetry followed by temperature programmed desorption			
	0.48 ± 0.01							
BET[b]	Surface area (m^2 g^{-1})		Pore volume (cm^3 g^{-1})		Pore size Å		Shows both micro- and mesoporosity	
	880.17		0.50		25.33			
TGA for coke content in spent catalyst (mass loss wt% in air) after different reaction temperatures	210 °C		Top	–	250 °C		Top	0.53
			Mid	–			Mid	0.48
			Bot	–			Bot	0.16
	230 °C		Top	0.39	270 °C		Top	0.46
			Mid	0.11			Mid	0.17
			Bot	0.20			Bot	0.11

[a] LPD Laboratory Services Ltd.

[b] MCA Services

although its stability was very good in comparison with its deactivation behaviour at lower temperatures.

The platinum dispersion of CBV712 determined by hydrogen chemisorption is given in Table 2. The low value (38.44 %) could have resulted from the formation of a considerably larger amount of coke, and it has been reported that the acid site density also affects the metal/acidity balance of the catalyst and metal dispersion, such that zeolites with Si/Al ratios between 15 and 40 had a good balance between the two functions and showed good stabilities [2].

Deactivation behaviour of CBV720 USY zeolite

CBV720 USY is obtained by steaming CBV600 for a second time at higher temperature and leaching with a mineral acid to produce the rest of the CBV-700 series, such as CBV740, CBV760 and CBV780. The preparation procedures performed by Zeolyst International are described by Remy et al. [20, 25]. Table 3 shows the in-house characterisation of CBV720 USY using various techniques.

Figure 7 shows TEM images of 1 wt% platinum loaded by an ion exchange method on CBV720 USY, and an identical activation method used during catalyst calcination by air and platinum reduction by pure hydrogen was used prior to the TEM analysis. A few very large (~25 nm) Pt particles were seen within the bulk of the zeolite support and at higher magnifications, Pt particles of 2 or 3 nm in diameter were seen in varying quantities throughout the USY support, with slightly smaller particles occurring at or near the surface.

The effect of TOS on C7 conversion, hydroisomerisation, hydrocracking and cyclic product yields at reaction temperatures ranging from 230 to 270 °C is shown in Fig. 8a–d, respectively.

Thirty minutes after the introduction of feed to the reactor, overall conversions were 11, 35, and 62 wt% at 230, 250 and 270 °C, respectively. At the lowest temperature of 230 °C, the catalyst lost about 1 wt% of its activity, and then reached a constant value after 60 h on stream. On the other hand, the deactivation rate of the fresh catalyst at 250 °C was slightly more rapid, as shown in Fig. 8a, with the overall conversion being 35 wt% 30 min after the introduction of feed to the reactor, decreasing with TOS to 33 wt% after 240 min, and then decreasing slowly, with the deactivation rate ranging from 1 to 2 wt% every 24 h until the reaction terminated, indicating reasonably good time stability. A rapid fall in catalyst activity occurred during the first few hours at the highest temperature of 270 °C, and then reached a constant deactivating value, ranging between 3 and 5 wt% every 24 h until the reaction terminated.

At the lower temperatures of 230 and 250 °C, selectivity towards hydroisomerisation products ranged from 97 to 98 % throughout the deactivation run, from the introduction of the feed to the reactor until both reactions terminated, while selectivity towards cracked products ranged from 0.05 to 0.4 % and from 0.04 to 0.3 %, respectively. Cyclic products reached high maximum values of 2.5 and 1 % at 230 and 250 °C, respectively, with the lowest value of 0.04 % observed at 270 °C. The maximum isomer yield obtained with the CBV720-based catalyst was around 61.8 wt% at 270 °C, where hydroisomerisation conversion was predominant. Cracked product selectivity increased initially at the higher temperatures of 250 and 270 °C during the initial few hours of the deactivation reaction, and then decreased rapidly throughout the TOS, such that selectivity of cyclic products was slightly higher at 230 and 250 °C than at the higher temperature of 270 °C.

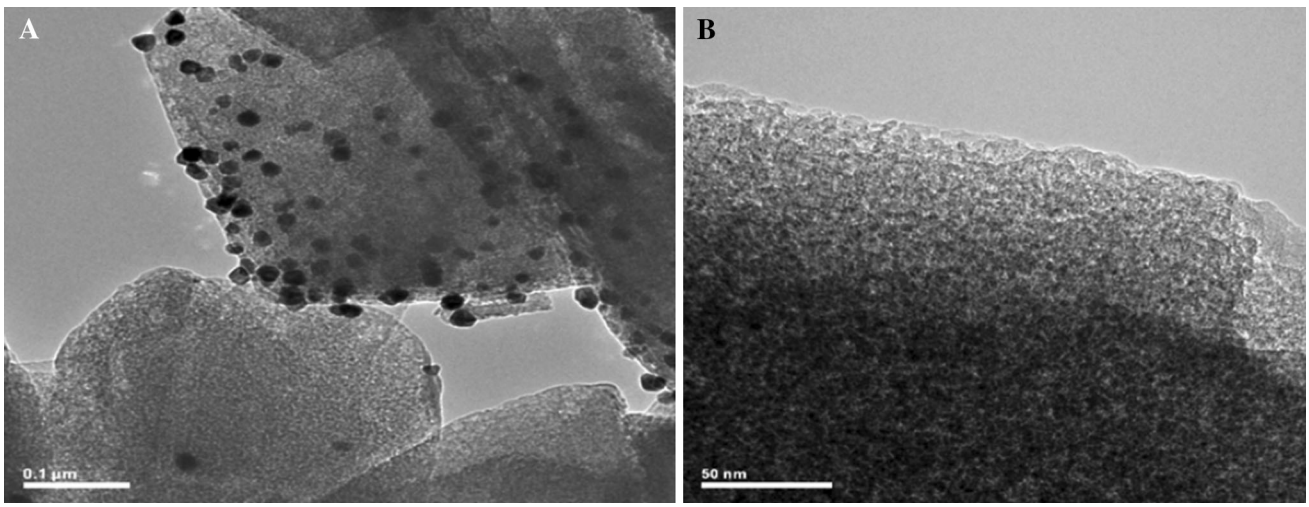

Fig. 7 TEM images of 1 wt% Pt/CBV720 USY

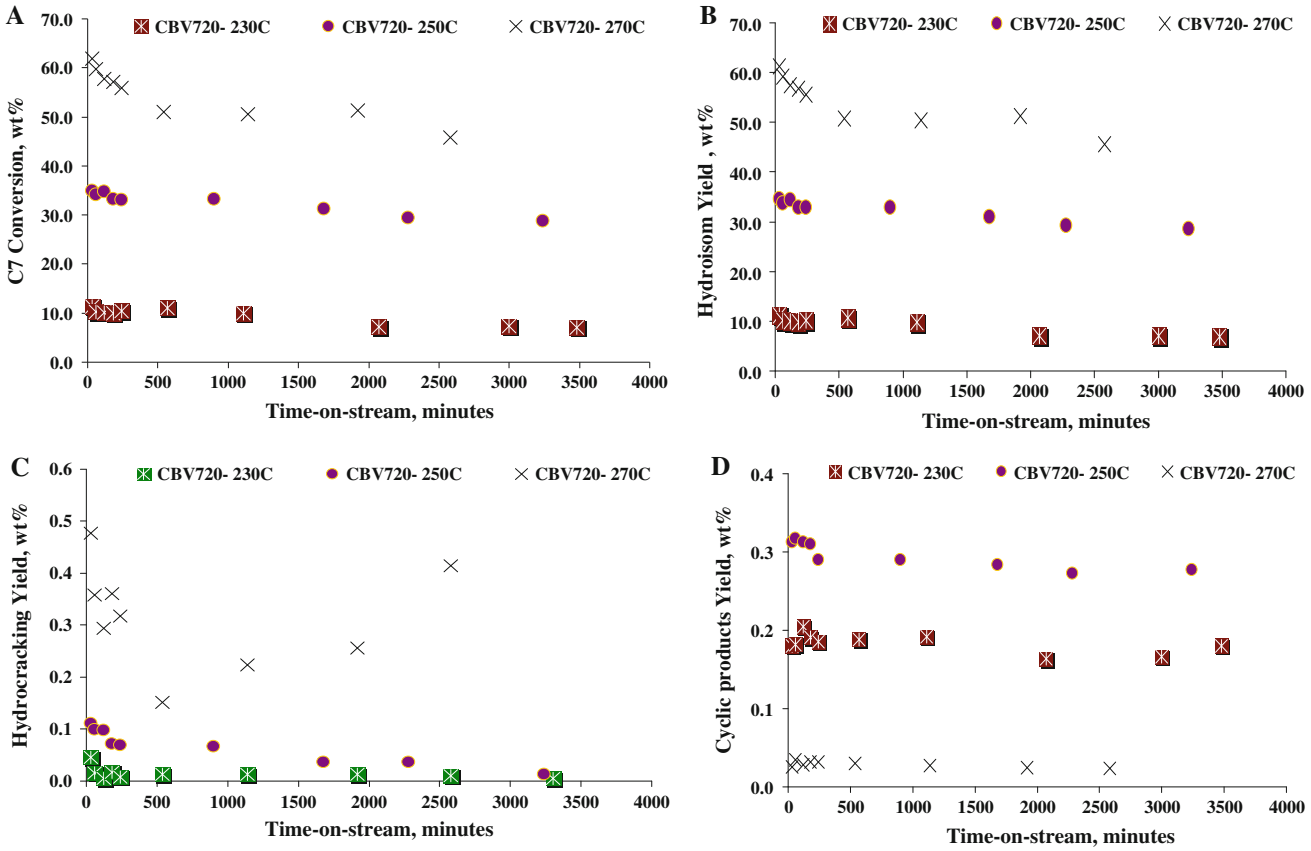

Fig. 8 Overall conversion (**a**), total yield of C7 isomers (mono + di + tribranched isomers) (**b**), total hydrocracking yield (**c**), and total yield of the cyclic products (**d**) as a function of TOS for CBV720 USY at various reaction temperatures

As CBV720 was produced via a severe dealumination process and leached by a mineral acid, the resultant catalyst has a small number of acid sites. This explains the lower activity of CBV720 accompanied by increased time stability compared with CBV712. Furthermore, removing the EFAL species by acid leaching, which can lead to enhanced acidity through the formation of Lewis acid sites, reduced the catalyst activity. Brønsted activity was predominant due to the stronger acid sites within the structure, and it has been hypothesised that these EFAL species increase the activity of the zeolite by stabilising the negative charge that is present in the zeolite structure after protons are removed, resulting in a synergy with nearby Brønsted acid sites and improved activity [26–28].

Due to the low acidity, there was less cracking activity, resulting in the catalyst having a higher stability against deactivation by coking, which is the case for zeolites with high Si/Al ratios [10, 12]. As with CBV712, it is obvious that the top zone had the highest hard coke content in the catalyst bed at each reaction temperature, whereas there was slightly less coke in the middle and bottom zones, as shown in Table 3. This suggests that the top zone of the catalyst bed contributed most activity and is where the reaction took place. In addition, the coke content in the top zone of this catalyst is much lower than in the case of CBV712, indicating the lower acidity of CBV720, which affects the stability of the catalyst, resulting in much slower deactivation and coke formation. In addition, the high surface area and large pore volume shown in Table 3, due to the more severe dealumination process and acid leaching, reduced the hard coke content and thus the deactivation rate.

The n_{Pt}/n_A ratio for CBV720 was calculated to be 0.115, indicating a balanced catalyst that performed as an 'ideal' hydroconversion catalyst. The high value of n_{Pt}/n_A meant that the number of chemical steps by which the cracked products could be generated and then oligomerated to form the coke-maker molecules was small, which in turn led to slower coke formation and higher catalyst stability. Despite large (~25 nm) Pt particles being seen within the surface of the catalyst support in the TEM images shown in Fig. 7, most of the Pt clusters, seen at higher magnifications, ranged between 2 and 3 nm across in varying quantities throughout the USY support, which indicates how well platinum is dispersed through the structure due to the cleaner pores and fewer EFAL species.

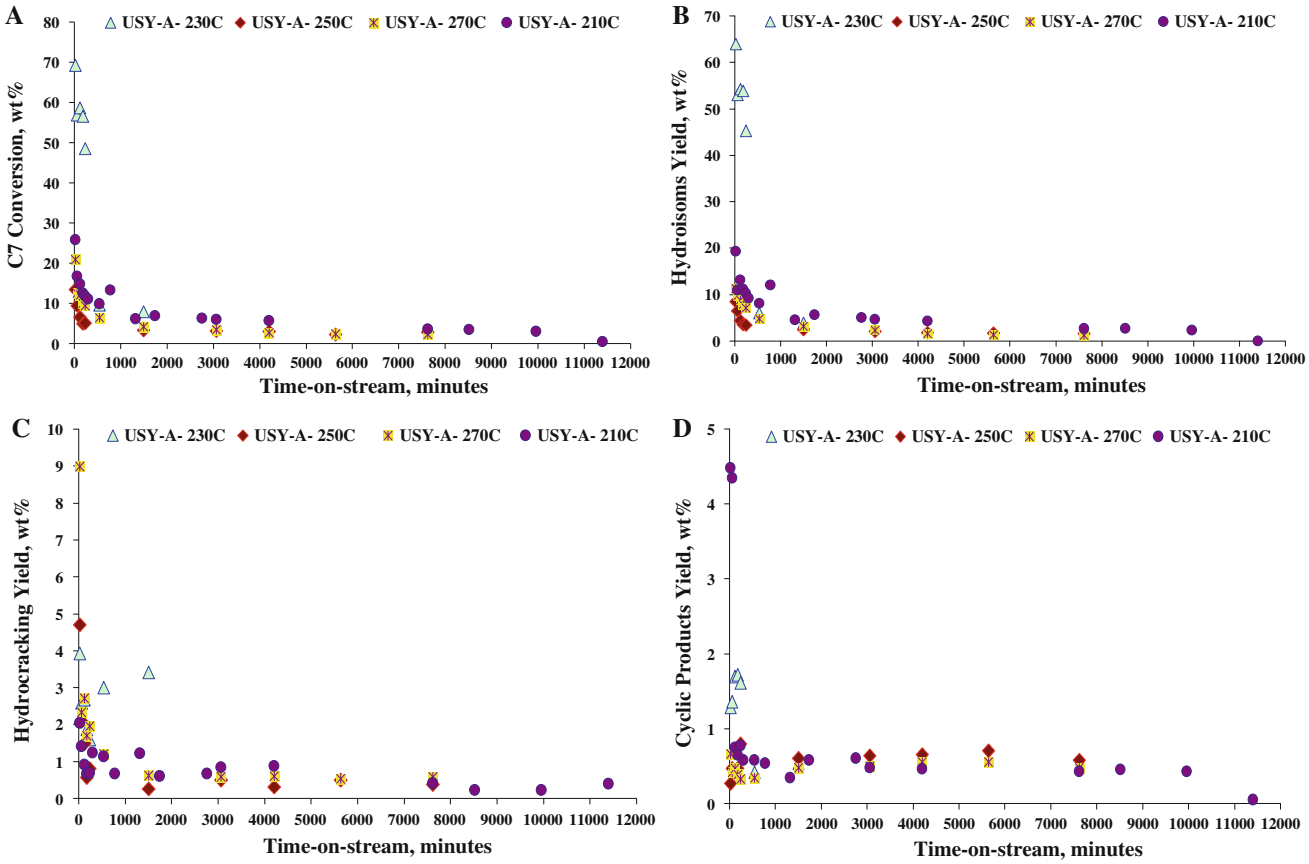

Fig. 9 Overall conversion (**a**), total yield of C7 isomers (mono + di + tribranched isomers) (**b**), total hydrocracking yield (**c**), total yield of the cyclic products (**d**) as a function of TOS for USY-A at various reaction temperatures

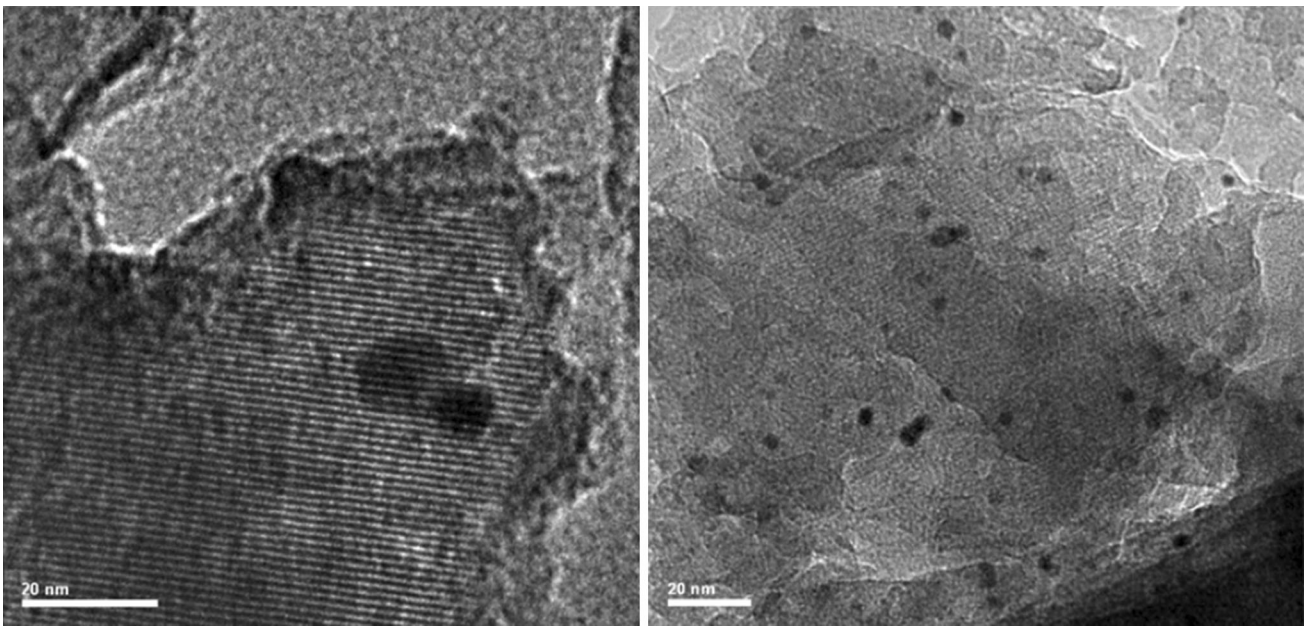

Fig. 10 TEM images for coked 1 wt% Pt/USY-A

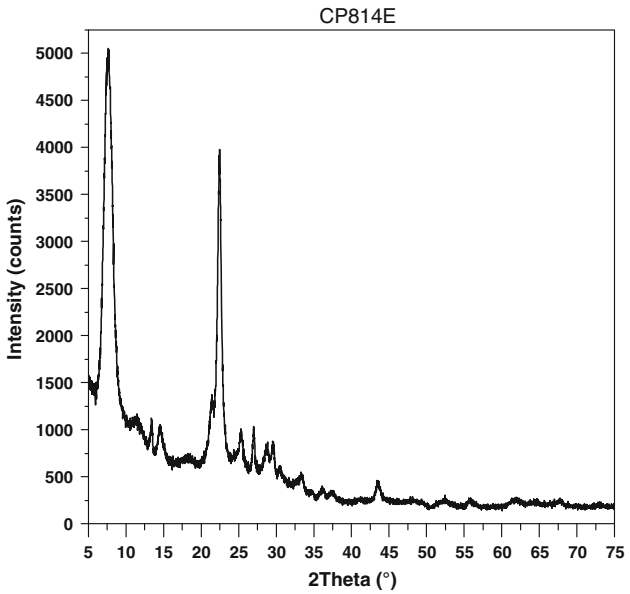

Fig. 11 XRD pattern of CP814E Beta

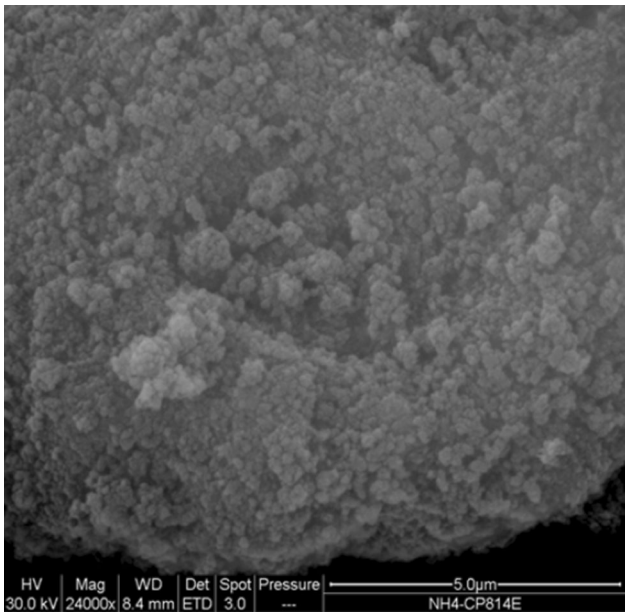

Fig. 12 SEM micrograph of CP814E Beta

Deactivation behaviour of USY-A zeolite

USY-A was synthesised using a pilot steaming rig supplied by the Crosfield company. Table 4 shows the in-house characterisation of USY-A using a variety of techniques. As this was a low Si/Al molar ratio catalyst, there were three chemical environments for Al confirming that USY-A was produced by a less severe dealumination process in order to achieve a lower Si/Al molar ratio and had not been acid-leached to remove EFAL species, giving it the same Si/Al ratio as via synthesis. Furthermore, four

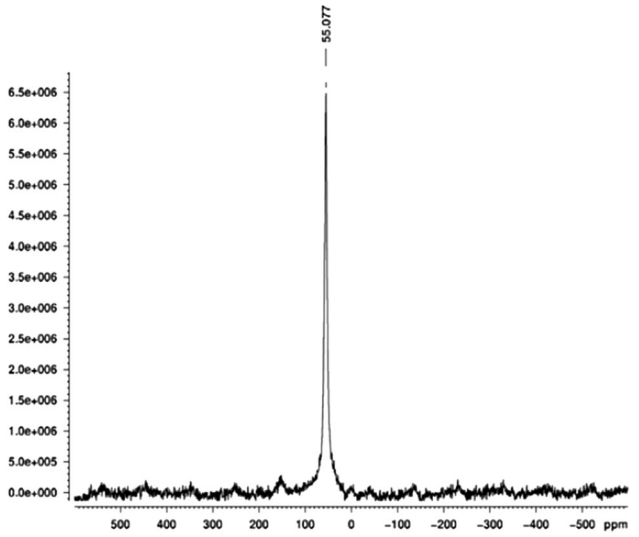

Fig. 13 ^{27}Al MAS NMR spectra of CP814E Beta

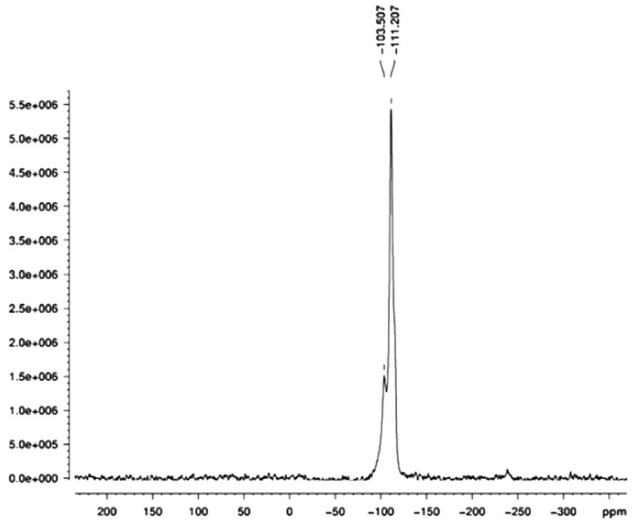

Fig. 14 ^{29}Si MAS NMR spectra of CP814E Beta

configurations of Si atoms were found within its structure, explaining the high total acidity for ammonia TPD.

The effect of TOS on the C7 conversion, hydroisomerisation, hydrocracking and cyclic product yields, respectively, at reaction temperatures of 210 to 270 °C, is shown in Fig. 9a–d, where the same amount of catalyst was used at each temperature.

Initially, the overall conversion at 210 °C was 25.8 wt% after 30 min, decreasing sharply with TOS to 9.87 wt% after 540 min. Conversion decreased steeply with a deactivation rate of around 2 to 0.46 wt% after 190 h, at which the 1 wt% Pt/USY-A was completely deactivated, as can be seen in Fig. 9a. The yields of isomers decreased more sharply from 19.26 wt% to approximately 8.58 wt% after 540 min on stream, then decreased slowly, whereas the

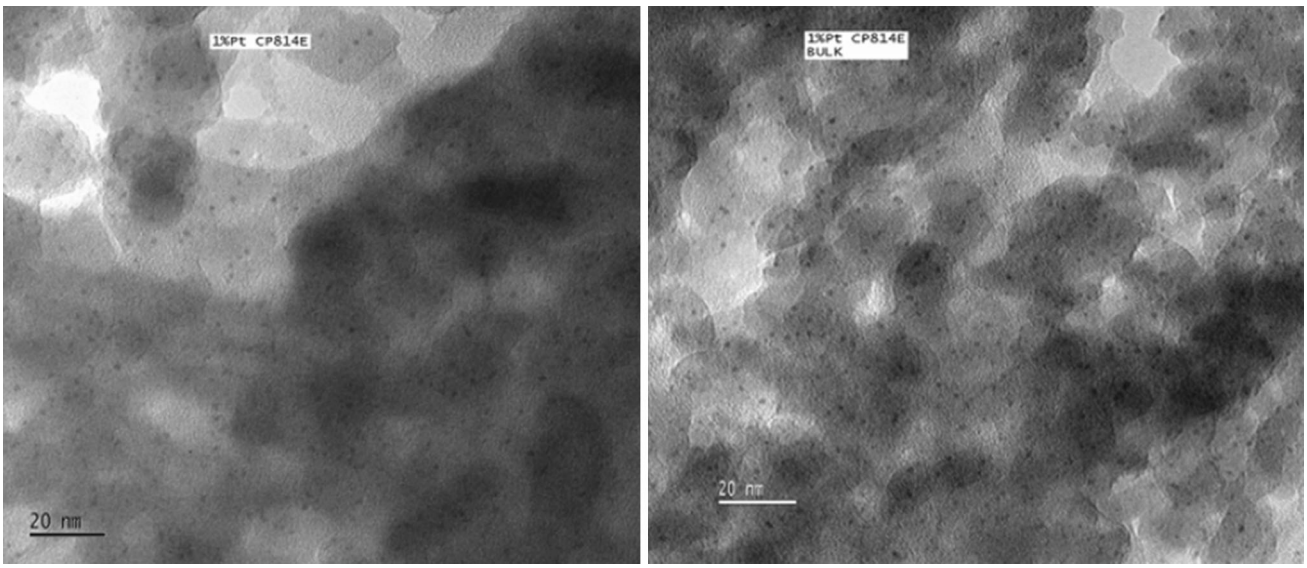

Fig. 15 TEM images of 1 wt% Pt/CP814E Beta

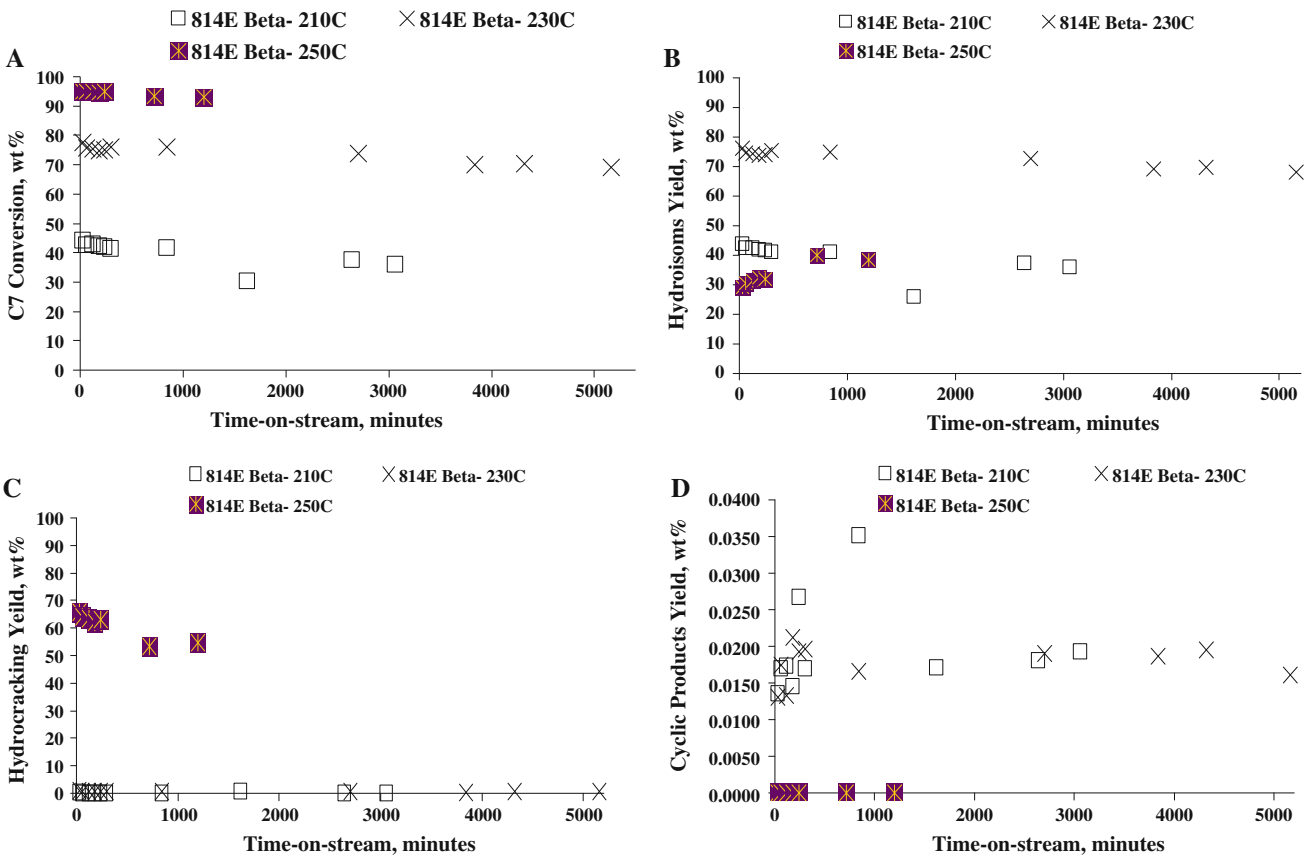

Fig. 16 Overall conversion (**a**), total yield of C7 isomers (mono + di + tribranched isomers) (**b**), total hydrocracking yield (**c**), and total yield of the cyclic products (**d**) as a function of TOS for CP814E at various reaction temperatures

yields of cracked products decreased more steeply with increasing TOS. The same TOS experiment was repeated after regenerating the catalyst and performed at the same reaction temperature of 210 °C for 166 h (approximately 7 days) in order to evaluate the stability of the catalyst against coking and to check its reversibility using the same reaction conditions; almost identical deactivation behaviour was recorded for this experiment. Significantly rapid

Table 4 In-house characterisation for USY-A

	Before ion exchange				After ion exchange with Pt precursor as tetramine platinum (II) chloride $(Pt(NH_3)_4Cl_2).H_2O$			
Elemental analysis (bulk)	Si/Al mole ratio		2.87		Si/Al mole ratio	2.87	Pt wt%	1.01
XPS[a] atomic % conc	Si	Al	Si/Al	Pt	Traces of Pt was found on the surface			
	24.07	10.86	2.22	0.03				
XRD	Crystallinity				Related to in-house as-synthesised Y			
	99.16							
NMR	Si/Al mole ratio for the framework				Four chemical environments for Si-NMR: Si(0Al), Si(1Al), Si(2Al) and Si(2Al)			
	7.11				Lewis acid sites existed: $Al(OSi)_4$, $(Al(H_2O)_5)^{3+}$ and $(Al(H_2O)_6)^{3+}$			
Pyridine-TPD/FTIR	Brønsted acid site concentration (B) (mmol g^{-1} $_{catalyst}$)				Lewis acid sites (L) concentration (mmol g^{-1} $_{catalyst}$)		L/B ratio	
	0.97				0.22		0.22	
Ammonia TPD	NH_3 desorption through TPD/mmol g^{-1}				Ammonia adsorption calorimetry followed by temperature programmed desorption			
	0.86 ± 0.01							
BET[b]	Surface area (m^2 g^{-1})		Pore volume (cm^3 g^{-1})		Pore size Å		Shows both micro- and mesoporosity	
	755.67		0.42		27.99			
TGA for coke content in spent catalyst (mass loss wt% in air)	Top				Mid		Bot	
	2.37				2.06		1.11	
	TGA analysis done after deactivation reactions at 210, 230, 250 and 270 °C							

[a] LPD Laboratory Services Ltd.

[b] MCA Services

deactivation behaviour occurred at the higher temperatures of 230 to 270 °C, with greater cracking activity during the initial few minutes, resulting in a very high rate of coke formation, which also accounted for the poor performance.

The higher concentration of Brønsted than Lewis acid sites resulted in a high total acidity and the predominance of Brønsted acidity, as shown in Table 4, meaning that cracking activity was high and coke formation very rapid during the initial few hours. It has been shown that the EFAL species generated during dealumination by steaming can be cationic, neutral, monomeric, oligomeric or polymeric and hydroxylated or not. These species can, therefore, either positively increase the acid strength by the interaction between bridging hydroxyl groups and neighbouring small EFAL species with Lewis acidity, or negatively by exchange of protonic sites (EFAL cationic species) and by pore blockage (polymeric species) [16].

Table 4 shows the TGA results for the hard coke content deposited over the aged USY-A top, middle, and bottom catalyst bed zones after unloading the spent catalyst from the atmospheric glass reactor and after the deactivation reactions at 210, 230, 250 and 270 °C. Coke was found predominantly in the top zone of the bed, suggesting pore blockage by excessive cracking (which probably occurred at higher temperatures) and reduced diffusion limitation compared with other zones.

As can be observed in Fig. 10, showing TEM images of spent USY-A, it is likely that the catalytic coke components were essentially formed and trapped within the channels of the catalyst micropores, so the first direct effect on the active sites was either by poisoning or by blocking of access to reactant molecules. Coke can also have an indirect effect, one that needs to be removed during catalyst regeneration and requires an oxidative treatment under severe conditions. This frequently has detrimental effects on the dealumination and degradation of the zeolite framework and the sintering of supported metals.

Some agglomerates of platinum particles can be observed within or upon the micropore channels of the coked USY-A, in Fig. 10, with the most likely explanation for this being catalyst regeneration prior to each deactivation run at each reaction temperature may have resulted in the sintering of supported platinum. Furthermore, as shown in the XPS analysis, some traces of platinum atoms were detected on the outer surface of the catalyst, indicating that some kind of agglomeration would have occurred towards the surface.

Table 5 In-house characterisation of CP814E Beta

	Before ion exchange				After ion exchange with Pt precursor as tetramine platinum (II) chloride $(Pt(NH_3)_4Cl_2).H_2O$			
Elemental analysis (bulk)	Si/Al mole ratio		13.21		Si/Al mole ratio	13.21	Pt wt%	1.07
XPS[a] atomic % conc	Si	Al	Si/Al	Pt	Pt was not found on the surface			
	25.77	2.39	10.78	0				
XRD	Crystallinity %				As was reported in the literature [8]			
	100							
NMR	Si/Al mole ratio for the framework				Two chemical environments for Si-NMR: Si(0Al) and Si(1Al)			
	13.45				Lewis acid sites are not present			
Ammonia TPD[b]	NH_3 desorption through TPD/mmol g^{-1}				Ammonia adsorption calorimetry followed by temperature programmed desorption			
	0.63 (± 0.01)							
Hydrogen chemisorption[b]	Metal dispersion %		Metallic surface area $m^2\ g^{-1}$ metal		Metallic surface area $m^2\ g^{-1}$ sample		Crystallite size, nm	
	30.67		75.74		0.81		3.69	
BET[b]	Surface area $m^2\ g^{-1}$		Pore volume $cm^3\ g^{-1}$		Pore size Å		Shows both micro- and mesoporosity	
	577.48		0.85		72.70			
TGA for coke content in spent catalyst (mass loss wt% in air) after various reaction temperatures	210 °C		Top	1.05	250 °C		Top	–
			Mid	0.20			Mid	–
			Bot	0.37			Bot	–
	230 °C		Top	0.85	270 °C		Top	–
			Mid	1.04			Mid	–
			Bot	0.94			Bot	–

[a] LPD Laboratory Services Ltd.

[b] MCA Services

Deactivation behaviour of CP814E beta zeolite

The XRD pattern for the fresh sample of CP814E (Fig. 11) is consistent with that reported in the literature for beta zeolite phase [21], and the SEM image of the sample (Fig. 12) shows nano-crystallites with no clear boundaries, and crystal particles clustered into agglomerates to form larger particles of different sizes. Similar observations on the CP814E morphology have been reported in the literature with the nano-sized crystals having different sizes depending on the synthesis or modification history [29, 30].

Figures 13 and 14 show the solid-state NMR spectra for ^{27}Al and ^{29}Si, respectively, with the NMR spectrum showing an ^{27}Al peak centred at 56.08 ppm in the region corresponding to the tetrahedrally coordinated aluminium, and no additional peaks were found which could be attributed to aluminium atoms in either octahedral or pentahedral coordinated EFALs. The ^{29}Si MAS NMR spectra (Fig. 14) shows two peaks at 111.21 and 103.51 ppm, which can be assigned to the Si(0Al) and Si(1Al) configurations, respectively, and the same spectral interpretation for both ^{27}Al and ^{29}Si MAS NMR has been reported in the literature [31, 32]. Moreover, as beta zeolite can be synthesised with Si/Al ratios between 10 and 100 [32], it can be concluded that CP814E is an as-synthesised beta zeolite and no post-synthesis modifications have been used [33]. Table 5 shows the in-house characterisation of CP814E using a range of different techniques. As shown in Table 5, a value of 13.45 was obtained for the framework Si/Al ratio using ^{29}Si MAS NMR, which concurred with the measurement given by chemical analysis of 13.21, which confirms that CP814E is an as-synthesised beta zeolite and no post-synthesis modification was used [33]. However, the Si/Al ratio of 10.78 on the surface (~5 nm) using XPS was significantly lower than the expected value of 13.45 as given in ^{29}Si MAS NMR or chemical analysis.

Since the metal cluster size in the bifunctional zeolite catalysts has a significant effect on the type of reaction catalysed by the metal function [34, 35], Fig. 15 shows TEM images of CP814E with 1 wt% platinum loaded by ion exchange. Prior to TEM analysis, activation and platinum reduction using air and hydrogen, respectively, were used to ensure comparable results with previous analyses. Fine platinum particles (~2 nm) could be seen within the grain of the beta zeolite support, even though hydrogen chemisorption indicated a low platinum dispersion as shown in Table 5. Furthermore, no platinum in the metallic

form could be seen on the catalyst subsurface (~5 nm), a fact that was confirmed by XPS.

The effect of TOS experiments on the C7 conversion, hydroisomerisation, hydrocracking, and cyclic product yields at different reaction temperatures from 210 to 250 °C is shown in Fig. 16a–d, respectively, with fresh catalyst used for each experimental run at the different reaction temperatures.

Initially, the overall conversion was 44, 77, and 95 wt% after 30 min from the point when the feed was introduced to the reactor at temperatures of 210, 230, and 250 °C, respectively. At 210 °C, the newly activated catalyst lost about 1–2 wt% of its activity and then reached a pseudo-stable state for the initial 60 min on stream. The initial conversion at 230 °C for the newly activated catalyst remained unchanged for about 2 days on stream, and then slightly decreased over time, with an overall conversion of 77 wt% after 30 min decreasing with the TOS to 74 wt% after 2,700 min, and then decreased slowly within the deactivation rate range of 1 to 2 wt% every 24 h until the reaction was finally terminated after about 86 h. On the other hand, the selectivity towards hydroisomerisation products was almost 99 % during the deactivation run at the 210 and 230 °C from the point of the feed being introduced into the reactor until both reactions terminated. In addition, selectivity towards cracked and cyclic products was very low, fluctuating in a very narrow range as a function of TOS in the range of 0.03 to 1 %.

It can be seen that CP814E (Fig. 16) demonstrated a significantly higher cracking activity at the reaction temperature of 250 °C than would be expected from its Si/Al ratio, with the initial conversion at 250 °C for the new activated catalyst being 95 wt% after 30 min, decreasing with the TOS to 93 wt% until the reaction was terminated after 2 days. The initial selectivity towards cracked products was high (70 %) compared to the hydroisomerisation products (30 %) for the C7 isomers. However, the cracking activity decreased with time and the C7 isomer production was seen to increase at the level-off stage, indicating that the reaction could not be conducted at temperatures higher than 270 °C as cracking activity would become the dominant reaction.

It has been reported that beta zeolite with a three-dimensional pore structure combined with no cavities or cages provided the best structure to resist deactivation due to coking with acid site density, metal/acidity balance and metal dispersion of the catalyst affecting the amount of coke deposited [2]. The methane-to-propane (C1/C3) ratio was employed as to provide an approximate measure of the activity of the metal function vs. acidic function, and is used in many industrial processes to follow the balance between activities of both functions. Methane is produced due to hydrogenolysis of the alkanes over the metal

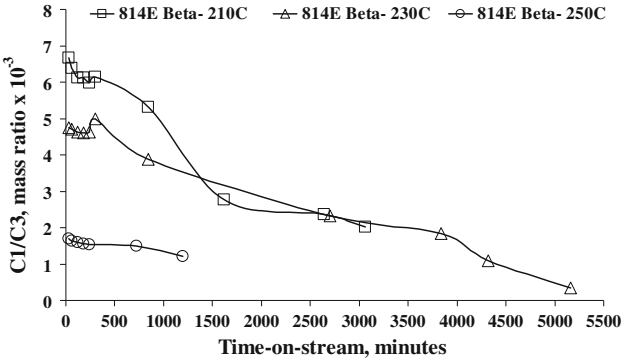

Fig. 17 Variation of the C1/C3 mass ratio as a function of TOS of CP814E

function whilst cracking on the acid sites produces propane almost exclusively [2]. The variation in C1/C3 mass ratio with TOS at various reaction temperatures is shown in Fig. 17, where the acid and metal functions were initially active at the temperatures of 210 and 230 °C, meaning that constant C1/C3 ratios were obtained. However, deactivation of the acid and metal functions caused the C1/C3 ratio to decrease rapidly, indicating a change in the balance between the two functions with TOS that may be due to the deposition of coke on both functions. The metal function deactivated faster than the acid function, though it was not significantly severe to cause a drop in *n*-C7 conversion.

The hard coke content shown in Table 5 at 210 and 230 °C was in the range of 0.2 and 1.05 wt%, indicating that the lower dispersions in CP814E result in the rate of deposition being strongly related to the initial activity of the acid function, the reaction temperature and the balance between the activities of metal and acid functions. CP814E loaded with 1 wt% Pt by ion exchange showed a low C1/C3 ratio indicating a good balance between the metal and acidic functions and thus it demonstrated satisfactory stability time.

Deactivation behaviour of some selected commercial mordenite zeolites

Figure 18a shows the SEM micrograms of CBV21A MOR. From the SEM images, it can be seen that CBV21A MOR contains larger crystallites up to 500 nm in length, accompanied by some smaller debris and agglomerates. The literature indicates that no synthesis route for nano-crystalline mordenite is so far available and that synthesis parameters such as silicon precursors, water content and $Na_2O/SiO_2/Al_2O_3$ ratios strongly affect mordenite morphology in terms of the size and aspect ratios of the crystals [36–38]. Figure 18b–d shows the SEM micrograms of 640HOA MOR, 660HOA MOR and 690HOA MOR,

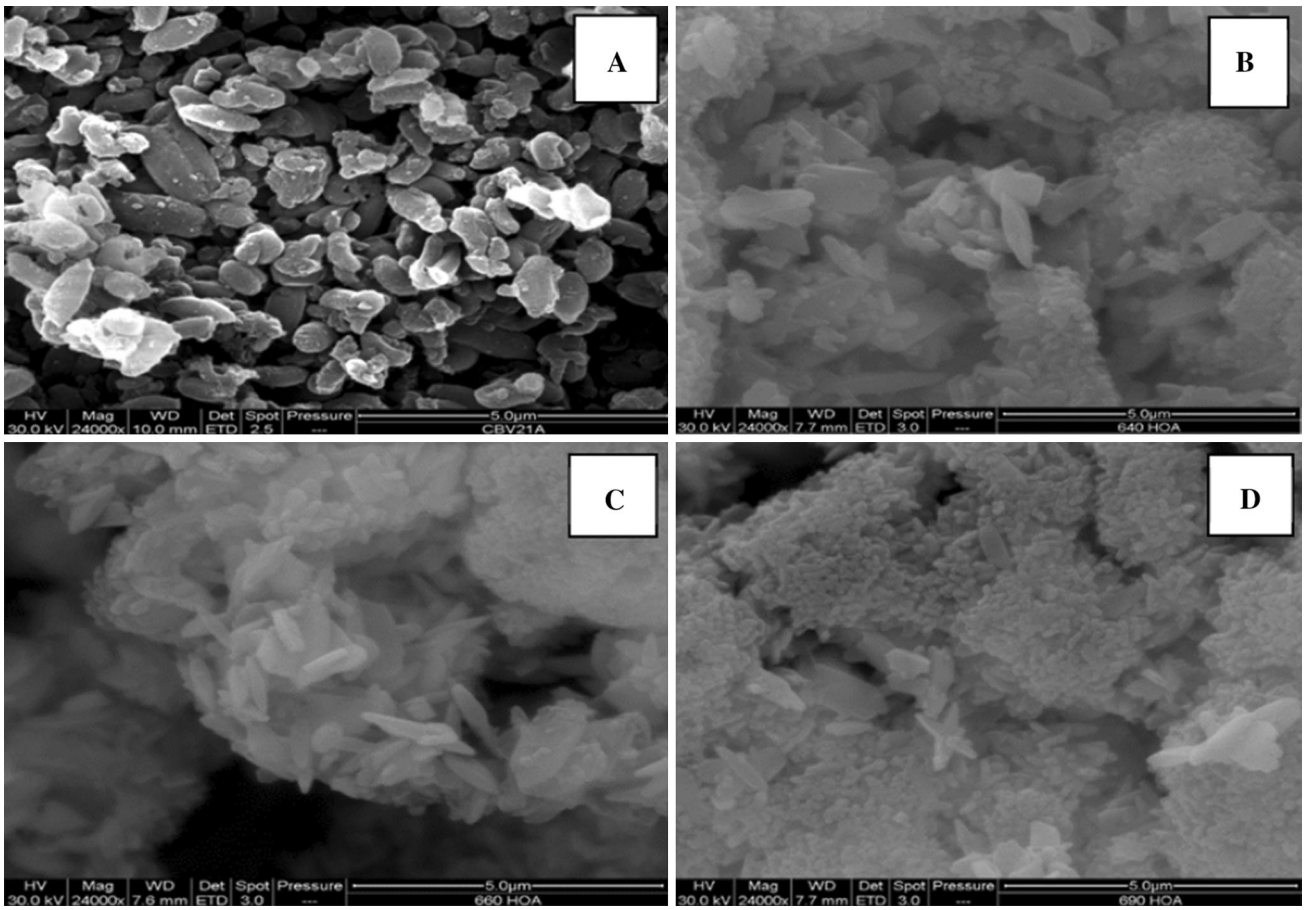

Fig. 18 SEM micrographs of CBV21A MOR (**a**), 640HOA MOR (**b**), 660HOA MOR (**c**) and 690HOA MOR (**d**)

respectively. From the SEM images, it can be seen that the catalysts contained sub-micron sized crystallites that had agglomerated into larger particles. Table 6 shows the in-house characterization of these catalysts using various different techniques. ^{27}Al and ^{29}Si solid-state NMR spectra for 640HOA, 660HOA and 690HOA catalysts have one ^{27}Al peak at about 55 ppm, which is assigned to tetrahedrally coordinated aluminium, with two more peaks that could be attributed to aluminium atoms as EFAL for 640HOA and 660HOA, whereas 690HOA showed no evidence of EFAL. This means that these three catalysts underwent dealumination of different severity, either by acid leaching, by steaming or both. In the ^{29}Si MAS NMR spectra, two peaks at about 112 and 106 ppm were assigned to Si(0Al) and Si(1Al) configurations, respectively. It is also evident that the intensity of the chemical environment of Si(0Al) increases as the Si/Al mole ratio increases and hence also as dealumination severity increases.

As dealuminated catalysts, they showed greater total pore volume, which means greater mesoporosity alongside the microporosity, hence larger surface area and smaller pore size compared with as-synthesised catalyst CBV21A MOR, as shown in Table 6. Furthermore, a good match was obtained for the Si/Al mole ratio of 690HOA by NMR and XPS, which supports the observation that there was no EFAL on the surface of this catalyst.

Well-dispersed platinum particles in the size range of 1–3 nm were obtained for the CBV21A MOR catalyst loaded with 1 wt% platinum by the ion exchange method. An activation method identical to that used during catalyst calcination by air and platinum reduction by pure hydrogen was used prior to the TEM analysis, as shown in the TEM images in Fig. 19.

TOS behaviour during C7 hydroisomerisation conversion was examined for the following commercial and in-house mordenite catalysts: CBV21A, 640HOA, 660HOA, and 690HOA. All of the above catalysts were loaded with 1 wt% Pt by the ion exchange method, as described above. Two very acidic commercial catalysts—1 wt% Pt/640HOA and 1 wt% Pt/660HOA deactivated very rapidly during the initial few seconds, due to a rapid coking that may have poisoned the acid sites of these catalysts and changed the effective acid site density needed for an ideal bifunctional conversion. As a consequence, no TOS results were reported for these catalysts. Figure 20 shows the effects of

Table 6 Characterization of zeolite MOR samples determined

Bulk (Si/Al) mol/mol	Framework (Si/Al) mol/mol	Crystallinity %	Bulk Pt wt%	(Si/Al) atomic conc % (XPS)	Pt Atomic Conc % (XPS)	Acidity mmol g^{-1}	Surface area m^2 g^{-1}	Pore volume cm^3 g^{-1}	Pore size Å
CBV21A MOR									
10.49	10.15	100	1.04	–	–	–	458.90	0.23	28.026
640HOA MOR									
–	12.0	100	–	–	–	–	–	–	–
660HOA MOR									
–	10.93	97	–	–	–	1.08	540.56	0.28	29.38
690HOA MOR									
114.38	17.88	108	0.97	16.50	0.04	0.10	559.94	0.28	24.48

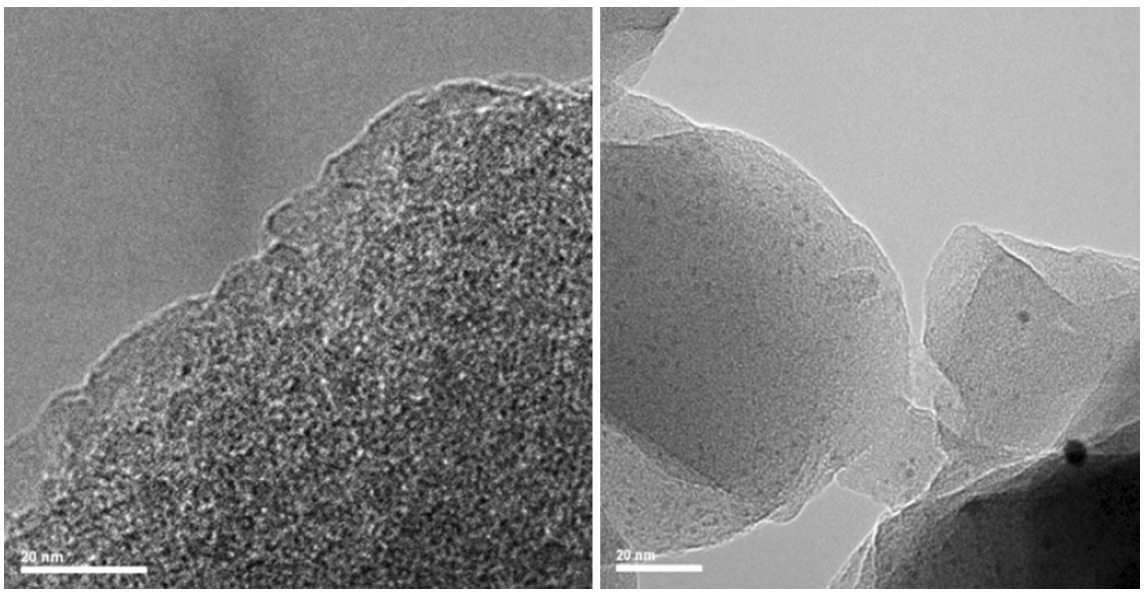

Fig. 19 TEM images of 1 wt% Pt/CBV21A MOR

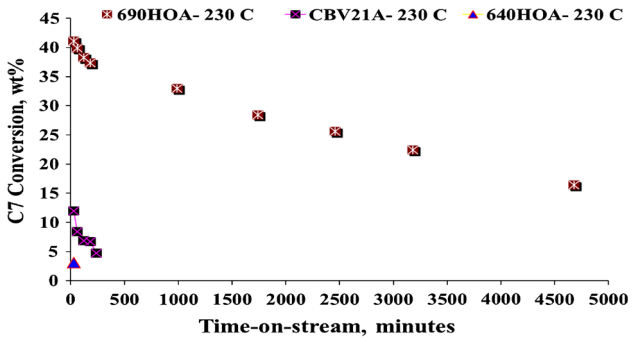

Fig. 20 Overall conversion as a function of TOS for commercial mordenite catalysts. WHSV = 5.13 h^{-1}; H_2/C7 (mol/mol) = 9; total pressure = 1 atm; temperature = 230 °C; 1 wt% Pt loading

TOS at a reaction temperature of 230 °C on C7 conversion, for the following catalysts: 1 wt% Pt/CBV21A and 1 wt% Pt/690HOA.

Initially, the overall conversions were 12, and 41 wt% after 60 min from the point when the feed was introduced to the reactor at 230 °C, for the 1 wt% Pt/CBV21A and 1 wt% Pt/690HOA mordenite catalysts, respectively. A rapid deactivation occurred for the 1 wt% Pt/CBV21A catalyst with high cracking activity, resulting in selectivity towards the cracked products at 24 %, compared with 71 % for the isomer products, and thereafter the catalyst was almost deactivated after 240 min on stream. On the other hand, greater TOS stability was shown by the 1 wt% Pt/690HOA mordenite catalyst. However, the 1 wt% Pt/690HOA catalyst deactivated continuously from the point when the feed was introduced to the reactor at the slower rate of 3–5 wt% every day, before achieving a pseudo-stable state at the end of the reaction. In addition, selectivity towards C7 isomers and cyclic products for both catalysts was in the range of 97–98 % and 2–3 %, respectively.

Faster deactivation and the mono-dimensional pore system of 1 wt% Pt/CBV21, coupled with a higher density of strong acid sites and as-synthesised zeolite, may have caused the lower activity, which may also be attributable to platinum crystallites blocking the pore openings, as previously reported [39, 40]. There are side pockets in the pore topology of mordenite that match the 12MR and 8MR crossing. The higher number of Brønsted acid sites in the cavities also increases the sensitivity of the 8 MR pores to coking and they can easily fill up and become blocked by carbonaceous deposits [41]. The average lifetime of the carbocations on the surface can be lengthened by strong acidity and narrow pore diameter, while the diffusion of the branched products can be slowed down. Each of these factors will help to crack the tertiary carbocations that have formed during isomerisation prior to desorption and will assist in the re-adsorption and cracking of the branched paraffins before they leave the pores and enter the gas stream [42].

There are various possible explanations for the slower deactivation of 1 wt% Pt/690HOA mordenite. First, it may be due to the medium acid strength of the catalysts and their reduced acid site density. Alternatively, it may be due to the balance between acid and metal active sites. It could also be ascribed to the existence of mesopores and to the slight increase in the pore volume, which may be beneficial to the diffusion of bulky moieties. Finally, it may be due to post-synthesised mordenite having smaller crystallites. The last two characteristics can be seen as reducing the resistance of the product molecules to formation and diffusion, resulting in less cracking and deactivation of the catalyst caused either by blockages at the site or by plugging of channels. The method of dealumination applied to the final lattice Si/Al ratio influences catalyst activity. For example, steam dealumination leaves the lattice with aluminium removed as EFAL, whereas samples that are practically free of EFAL can result from acid leaching, so EFAL may have a negative effect by blocking pores and preventing the Pt from being well dispersed during the ion exchange process. This may explain the deactivation of the 1 wt% Pt/690HOA steamed mordenite catalysts.

Conclusion

It can be concluded from this investigation of the deactivation of a range of commercial bifunctional nanoporous-based catalysts during the hydroisomerisation of normal heptane (*n*-C7) under identical reaction conditions. The main cause of deactivation of acid zeolite catalysts is generally coking, as coke compounds become trapped in the zeolite pores and can poison the acid sites or block their access. Two factors have been found to affect strongly the rate of coke formation: the structure and openings of the pores, and the density of strongly acid sites. There is a clear correlation between the yield of cracked products obtained, the existence of stronger acid sites and the formation of hard coke. Thus, lower acidity results in the catalyst being more stable against deactivation by coking, which is the case for zeolites with high Si/Al ratios and those which have been acid-leached. The number of strong acid sites can be reduced by dealumination and acid leaching, thus increasing mesoporosity inside the zeolite crystallites and so reducing the limitations to diffusion, resulting in shorter residence times, which facilitates desorption of the products. Furthermore, the balance between the number of metal sites and the number of acid sites plays an important role in determining the activity, selectivity and stability of bifunctional catalysts.

It was found that zeolites with channel intersection cavities of comparable size to their apertures, like zeolite beta, were minimally affected by coke formation; thus the size of the channel intersection should be only slightly larger than that of the zeolite aperture, such that the coke precursors are unable to remain trapped inside the cavities and form bulky carbonaceous compounds. On the other hand, coke precursors can be trapped and become enlarged in the supercages, thus blocking the pores of a catalyst such as zeolite Y, which has relatively large cavities or supercages in comparison with the openings of the channels. Moreover, zeolites with nano-crystalline structures are more stable with respect to coking and have better TOS behaviour, due to the shorter time it takes reactants and products to diffuse into and out of the smaller crystals in the structure.

References

1. Guisnet M, Costa L, Ribeiro FR (2009) Prevention of zeolite deactivation by coking. J Mol Catal A Chem 305:69–83
2. Gopal S (2003) Synthesis, Modification, Characterization and Catalytic Studies of Zeolite based Bifunctional Catalysts for Hydroisomerization Reactions. Dissertation, University of Cincinnati, Cincinnati, Ohio
3. Rollmann LD (1977) Systematics of shape selectivity in common zeolites. J Catal 47:113–121
4. Rollmann LD, Walsh DE (1979) Shape selectivity and carbon formation in zeolites. J Catal 56:139–140
5. Guisnet M, Magnoux P (1989) Coking and deactivation of zeolites—influence of the pore structure. Appl Catal 54:1–27
6. Guisnet M, Magnoux P (1992) Composition of the carbonaceous compounds responsible for zeolite deactivation—modes of formation. Zeolite Microporous Solids Synth Struct React 352: 437–456

7. Gopal S, Smirniotis PG (2002) Deactivation behavior of bifunctional Pt/H-zeolite catalysts during cyclopentane hydroconversion. J Catal 205:231–243
8. Zhang W, Smirniotis PG (1998) Dealuminated zeolite-based composite catalysts for reforming of an industrial naphthene-rich feedstock. Appl Catal A 168:113–130
9. Walsh DE, Rollmann LD (1977) Radiotracer experiments on carbon formation in zeolites. Effect of aromatic content of hydrocarbon mixtures. J Catal 49:367–375
10. Stöcker M (2005) Gas phase catalysis by zeolites. Microporous Mesoporous Mater 82:257–292
11. Sie ST (2008) Isomerization. In: Ertl G, Knözinger H, Schueth F, Weitkamp J (eds) Handbook of Heterogeneous Catalysis, 2nd edn. Wiley-VCH Verlag GmbH, Weinheim, pp 2809–2829
12. Akhmedov VM, Al-Khowaiter SH (2007) Recent advances and future aspects in the selective isomerization of high *n*-alkanes. Catal Rev 49:33–139
13. Guisnet M, Ribeiro FR (2011) Deactivation and regeneration of zeolite catalysts. Imperial College Press, London
14. Zeolyst International. http://www.zeolyst.com/our-products/standard-zeolite-powders/zeolite-y.aspx. Accessed 29 May 2011
15. Tosoh Corporation. http://www.tosoh.com/Products/tcdzeo.htm#hzc. Accessed 26 June 2011
16. Rawlence DJ, Earl GJ (1993) Materials having novel structure factors for catalysis of hydrocarbon transformation and development of selective processes. BRITE-EURAM 4633, 5th Meeting Report, Elf Solaize
17. Abudawood R, Alotaibi F, Garforth A (2011) Hydroisomerization of *n*-heptane over Pt-loaded USY zeolites. Effect of steaming, dealumination and the resulting structure on catalytic properties. Ind Eng Chem Res 50:9918–9924
18. Abudawood R (2010) Hydroisomerization of Alkanes over Metal-Loaded Zeolite Catalysts. Dissertation, University of Manchester
19. Weisz PB, Frilette VJ (2002) Intracrystalline and molecular-shape-selective catalysis by zeolite salts. J Phys Chem 64:382
20. Remy MJ, Stanica D, Poncelet G, Feijen EJP, Grobet PJ, Martens JA, Jacobs PA (1996) Dealuminated H–Y zeolites: relation between physicochemical properties and catalytic activity in heptane and decane isomerization. J Phys Chem 100: 12440–12447
21. Treacy MMJ, Higgins JB (2001) Collection of simulated XRD powder patterns for zeolites. Elsevier, Amsterdam
22. Guisnet M, Ribeiro FR (2011) Deactivation and regeneration of zeolite catalysts. Imperial College Press, London, pp 204–205
23. Guisnet M, Alvarez F, Giannetto G, Perot G (1987) Hydroisomerization and hydrocracking of *n*-heptane on PtHzeolites. Effect of the porosity and of the distribution of metallic and acid sites. Catal Today l:415–433
24. Alvarez F, Rebeiro FR, Perot G, Thomazeau C, Guisnet M (1996) Hydroisomerization and hydrocracking of alkanes—7. Influence of the balance between acid and hydrogenating functions on the transformation of *n*-decane on PtHY catalysts. J Catal 162: 179–189
25. Morin S, Ayrault P, Gnep NS, Guisnet M (1998) Influence of the framework composition of commercial HFAU zeolites on their activity and selectivity in *m*-xylene transformation. Appl Catal A 166:281–292
26. Alvarez F, Giannetto G, Guisnet M, Perot G (1987) Hydroisomerization and hydrocracking of *n*-alkanes: 2. *n*-Heptane transformation on a Pt-dealuminated Y zeolite—comparison with a Pt-Y zeolite. Appl Catal 34:353–365
27. Gauw F (2002) Kinetic Studies of Alkane Hydroisomerization over Solid Acid Catalysts. Dissertation, Eindhoven University of Technology
28. Guisnet M, Ribeiro FR (2011) Deactivation and regeneration of zeolite catalysts. Imperial College Press, London, p 27
29. Petushkov A, Giorvanni M, Larsen SC (2011) From nanoparticles to hierarchical structures: controlling the morphology of zeolite beta. Microporous Mesoporous Mater 143:97–910
30. Trombetta M, Busca G, Storaro L, Lenarda M, Casagrande M, Zambon A (2000) Surface acidity modifications induced by thermal treatments and acid leaching on microcrystalline H-BEA zeolite. A FTIR, XRD and MAS-NMR study. Phys Chem Chem Phys 2:3529–3537
31. Maier SM, Jentys A, Lercher JA (2011) Steaming of zeolite BEA and its effect on acidity: a comparative NMR and IR spectroscopic study. J Phys Chem 15:8005–8013
32. Park JN, Wang J, Hong SI, Lee CW (2005) Effect of dealumination of zeolite catalysts on methylation of 2-methylnaphthalene in a high-pressure fixed-bed flow reactor. Appl Catal A 292:68–75
33. Jia C, Massiani P, Barthomeuf DJ (1993) Characterization by infrared and nuclear magnetic resonance spectroscopies of calcined beta zeolite. Chem Soc Faraday Trans 89:3659–3665
34. Blomsma E, Martens JA, Jacobs PA (1997) Isomerization and hydrocracking of heptane over bimetallic bifunctional PtPd/H-beta and PtPd/USY zeolite catalysts. J Catal 165:241–248
35. Bowen TC, Vane LM (2006) Ethanol, acetic acid, and water adsorption from binary and ternary liquid mixtures on high-silica zeolites. Langmuir 22:3721–3727
36. Van Laak ANC, Sagala SL, Zečević J, Friedrich H, de Jongh PE, de Jong KP (2010) Mesoporous mordenites obtained by sequential acid and alkaline treatments—catalysts for cumene production with enhanced accessibility. J Catal 276:170–180
37. Zhang L, van Laak ANC, de Jongh PE, de Jongh KP (2009) Synthesis of large mordenite crystals with different aspect ratios. Microporous Mesoporous Mater 126:115–124
38. Van Laak ANC (2011) Post-Synthesis Modifications on Zeolites for Improved Accessibility and Catalytic Performance. Dissertation, Utrecht University
39. Wang ZB, Kamo A, Yoneda T, Komatsu T, Yashima T (1997) Isomerization of *n*-heptane over Pt-loaded zeolite/beta catalysts. Appl Catal 159:119–132
40. Lee JK, Rhee HK (1997) Characteristics of Pt/H-beta and Pt/H-mordenite catalysts for the isomerization of *n*-hexane. Catal Today 38:235–242
41. Van Donk S (2002). Adsorption, Diffusion and Reaction Studies of Hydrocarbons on Zeolite Catalysts. Dissertation, Utrecht University
42. Chica A, Corma A, Miguel PJ (2001) Isomerization of C5–C7 *n*-alkanes on unidirectional large pore zeolites: activity, selectivity and adsorption features. Catal Today 65:101–110